Science of the Total Environment 912 (2024) 168970

Contents lists available at ScienceDirect

Science of the Total Environment

journal homepage: www.elsevier.com/locate/scitotenv

# Formation kinetics of SVOC organic films and their impact on child exposure in indoor environments

Zhuo Chen [b], Yilun Gao [b], Fanxuan Xia [b], Chenyang Bi [c], Jinhan Mo [a,b,d,e,f,*]

[a] College of Civil and Transportation Engineering, Shenzhen University, Shenzhen 518060, China
[b] Beijing Key Laboratory of Indoor Air Quality Evaluation and Control, Department of Building Science, Tsinghua University, Beijing 100084, China
[c] Aerodyne Research Inc., Billerica, Massachusetts, 01821, USA
[d] Key Laboratory of Coastal Urban Resilient Infrastructures (Shenzhen University), Ministry of Education, Shenzhen 518060, China
[e] Key Laboratory of Eco Planning & Green Building (Tsinghua University), Ministry of Education, Beijing 100084, China
[f] State Key Laboratory of Subtropical Building and Urban Science, Guangzhou 510641, China

## HIGHLIGHTS

- A model was developed to predict the partition coefficients of organic films.
- Indoor distributions of SVOCs with different physical properties were determined.
- Effects of particle deposition and film $K_{om}$ were analyzed for organic-film growth.
- The influence of SVOC-film ingestion on children's exposure was estimated.

## GRAPHICAL ABSTRACT

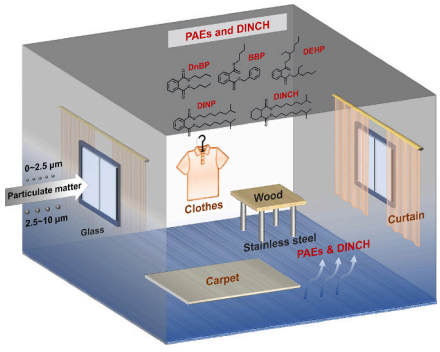


## ARTICLE INFO

Editor: Hai Guo

*Keywords:*
Indoor air quality
Semivolatile organic compounds
Organic film
Partition coefficient
Exposure assessment

## ABSTRACT

We conducted an SVOC mass transfer and child-exposure modeling analysis considering the combined sorption of multiple SVOCs containing DnBP, BBP, DEHP, DINP and DINCH in indoor environments. A mechanistic model was applied to describe the organic film formation, and a partition-coefficient-prediction model was originally developed for the realistic organic films. The characteristics of film formation on impermeable surfaces were examined based on three different assumptions: the widely-used constant $K_{ns,im}$ assumption, $K_{oa}$ assumption, and the proposed $K_{om}$ assumption (predicted specifically for the realistic organic films in this study). After long-term SVOC sorption, the organic film reached increasing equilibrium gradually under constant $K_{ns,im}$ assumption. While under $K_{oa}$ and $K_{om}$ assumption, organic films exhibited nearly linear increases on surfaces, the trends of which agreed well with field studies. However, the film thicknesses calculated under $K_{om}$ assumption with larger film partition coefficients were approximately twice larger than those under $K_{oa}$ assumption. Meanwhile, Horizontal surfaces with higher deposition rates of particle-phase SVOCs exhibited larger velocities of film growth compared to vertical surfaces. Under the $K_{om}$ assumption, exposures of hazardous SVOCs for a 3-year-old child increased by 87.5 %–198.7 % even with the weekly cleaning of indoor impermeable surfaces, carpet and cloth.

* Corresponding author at: College of Civil and Transportation Engineering, Shenzhen University, Shenzhen 518060, China.
*E-mail address:* mojinhan@szu.edu.cn (J. Mo).

https://doi.org/10.1016/j.scitotenv.2023.168970
Received 21 August 2023; Received in revised form 8 November 2023; Accepted 27 November 2023
Available online 2 December 2023

This study is anticipated to provide valuable insights into the film-forming characteristics of multiple SVOCs and the accompanying significant health risks to human beings in indoor environments.

## 1. Introduction

Phthalate esters (PAEs), a type of toxic semi-volatile organic compounds (SVOCs) (Liu et al., 2020), are widely found indoors (Zhang et al., 2020). There are also large amounts of airborne particles and dust in indoor environments (Gao et al., 2023; Gao et al., 2022; Tian et al., 2023). Due to the strong sorption capacities of PAEs on indoor surfaces, airborne particles and settled dust (EPA, 2011), PAEs can easily be ingested by humans through hand contact and mouthing, which can cause severe health risks (Bolling et al., 2020; Golestanzadeh et al., 2020). With the raising attention on the hazards of PAEs, diisononyl cyclohexane-1,2-dicarboxylate (DINCH) has emerged as a widely-used alternative for PAEs in application (Schossler et al., 2011). However, DINCH also has a strong sorption capacity similar to PAEs due to its large molecular weight (424.7 g/mol) and low vapor pressure ($8.9 \times 10^{-5}$ Pa) (Rodriguez-Carmona et al., 2019). As a result, humans can potentially be exposed to DINCH by mouthing contaminated surfaces and particulate matter, which then poses potential health risks (Fromme et al., 2016).

As explored in previous studies, organic pollutants with strong sorption capacities, such as PAEs and DINCH, can continuously accumulate on impermeable surfaces indoors to form organic films (Chen et al., 2022b). This phenomenon has been widely reported in the literature in the field of indoor environmental research. For instance, Liu et al. (2003) identified polar organic compounds on indoor glass windows, including n-alkane, monoacids and diacids. Huo et al. (2016) traced the PAE film growing processes during summer and winter, and further evaluated the implications for human exposure. Wang et al. (2021) conducted an in-depth investigation on PAE distributions in glass window films in university dormitories in Beijing, and they further analyzed the key environmental factors that influenced film formation (Fan et al., 2023). The organic film will form on the surfaces owing to the combined effects of adsorption to absorption, and further enhance the mass transfer rate to enrich more pollutants (Chen et al., 2023; Chen et al., 2022a). To sum up, it is demonstrated that organic films can sustainably enrich indoor organic pollutants, thereby forming combined pollution to pose a greater health risk to human beings. Consequently, it is crucial to establish an accurate model that describes the combined sorption of organic compounds and the formation of organic films, and then evaluates the human-organic-film exposures in indoor environments. Further investigations in this research field are warranted.

Several studies have focused on the fate and transport modeling of PAEs in indoor environments. Bennett and Furtaw (2004) presented a dynamic mass-balance compartment model based on fugacity principles to predict the pesticide concentration in a home. Weschler and Nazaroff (2008) gave a schematic illustration of key aspects of indoor SVOC dynamics. Further, they assessed the time scales for SVOCs to achieve equilibrium sorption on surfaces and airborne particles under the constant SVOC mass flow rate assumption. Xu et al. (2009) developed a concentration-driven model based on the mass transfer principle to predict the PAE distributions in residential buildings, in which the particle mass concentrations were assumed as constants without further modeling the particle transport dynamics. Based on Xu's study, Liu et al. (2010) developed a dynamic mass transfer model for airborne particles. Shi and Zhao optimized the SVOC sorption models on airborne particles (Shi and Zhao, 2014) and settled dust (Shi and Zhao, 2015). Liang et al. (2019) summarized the modifications above in their models and further raised a reasonable assumption that the gas-phase SVOC concentrations adjacent to surface and dust are the same in value. Nevertheless, the SVOC sorption process on indoor surfaces was hypothesized as monolayer adsorption with constant surface partition coefficients. The SVOC partition coefficients were obtained from the studies that determined the partition coefficients of impermeable surfaces with different textures in an experimental way (Liang and Xu, 2014b; Wu et al., 2017; Xu et al., 2009). For instance, Wu et al. (2017) characterized the DEHP partition coefficients on surfaces such as aluminum, stainless steel, steel, ground glass and acrylic, with respective values of $6 \times 10^2$ m, $1.2 \times 10^3$ m, $1.0 \times 10^4$ m, $4.2 \times 10^3$ m and $5 \times 10^2$ m. It should be noted that the SVOC adsorption experiments were conducted under ideal experimental conditions, where the target substrates were exposed only to a single gaseous SVOC without any other organic pollutant present. The hypothesis is suitable for the laboratory scenario but may introduce errors for the real-environment modeling.

In order to describe the growth of organic film on surfaces, some studies have spent their effort to develop models for surface film formation dynamics (Eichler et al., 2019; Lakey et al., 2021; Weschler and Nazaroff, 2017). Weschler and Nazaroff (2017) presented a model for the growth of organic films on impermeable indoor surfaces, assuming the gas-phase SVOCs absorb in the pre-existing films. Eichler et al. (2019) further summarized the key mechanisms of film formation and provided a detailed model for SVOC sorption processes, encompassing adsorption to absorption. Lakey et al. (2021) developed a kinetic multilayer model of film formation (KM-FILM) that fully followed the Langmuir and Brunauer-Emmett-Teller (BET) theories, and the results agreed well with those of a chamber study (Eichler et al., 2018). Nevertheless, there are still some research gaps in the reported film-forming models. Firstly, the models were developed under ideal cases, assuming that the gas-phase SVOC adsorption was the only factor for organic-film formation and the gas-phase SVOC concentrations were constants. Secondly, the octanol-air partition coefficient ($K_{oa}$) was simplified as the film partition coefficient in the reported models, hypothesizing the organic films are similar to octanol in affinity. It simplifies the determinations of SVOC partition coefficients in films but may potentially introduce errors in estimating SVOC concentration distribution due to neglecting the influence of film components on the SVOC sorption capacity. Human exposure to SVOCs resulting from organic film ingestion is also well worth quantifying. According to Zartarian et al.'s (1997) studies, children tend to continually touch and mouth polluted indoor surfaces, with a large possibility of ingesting abundant organic films and then causing severe health risks. Zhang et al. (2014, 2009) developed the Indoor Chemical Exposure Classification/Ranking Model (ICECRM) that was applied to human exposure assessment through different pathways, including organic film ingestion. Li et al. (2018) further built the Risk Assessment, IDentification And Ranking-Indoor and Consumer Exposure (RAIDAR-ICE) model based on ICECRM, which also described the ingestion of organic films. Therefore, we intend to investigate the critical factors that dominate the film formations and the associated exposure aggravations for children in indoor environments.

To fill the research gaps, we modeled the organic film formation in realistic indoor environments considering multiple SVOC mass-flux factors like the convection in the gas phase and deposition and resuspension in the particle phase. The emission and combined sorption of multiple SVOCs are described in the mechanistic model, and five typical SVOCs, including DnBP, BBP, DEHP, DINP and DINCH are selected as target SVOCs for their wide distributions indoors (Eichler et al., 2018; Liang and Xu, 2014a; Liang and Xu, 2014b). Using molecular dynamics simulation, we also developed a partition-coefficient predicting model for the realistic organic films. After quantifying the SVOC distributions, we further conducted a scenario analysis to estimate the SVOC exposures of a 3-year-old child, aiming to explore the influence of film formations on SVOC intakes. The objectives of this research are as follows: (1) developing a partition-coefficient predicting model to estimate the film partition coefficients of the realistic organic films; (2) determining

the distributions of SVOCs with different physicochemical properties in indoor environments, especially on indoor surfaces; (3) investigating the characteristics of organic-film formation on indoor surfaces and identifying the critical factors that dominate this process; (4) estimating the influence of SVOC-film formations on the exposure of children. We aim to enhance the understanding of SVOC behavior in indoor environments by addressing these aims and providing valuable insights for assessing human exposure risks.

## 2. Methodology

### 2.1. Mass transfer model of PAEs in a residence

A mass transfer model was developed to study the emission and combined sorption of multiple SVOCs (DnBP, BBP, DEHP, DINP and DINCH) in indoor environments. The model, illustrated in Fig. 1, incorporates the mass conservations of particulate matter and organic pollutants to govern their indoor concentration distributions. Particulate matter is introduced into indoor air through ventilation to form indoor airborne particles. These particles can be deposited on indoor surfaces to form settled dust. The model accounts for both impermeable and permeable surfaces within the indoor environment. The SVOC mass transfer process is coupled with airborne particles and settled dust distributions through sorption. Initially, SVOCs are released from source materials to indoor air or settled dust. The gaseous SVOCs would further be adsorbed on airborne particles, impermeable/permeable surfaces and settled dust. Meanwhile, there are mass exchanges between particle- and dust-phase SVOCs through deposition and resuspension. Due to the SVOC combined sorption, organic films are expected to be formed on indoor impermeable surfaces, resulting in continuous SVOC sorption in films and an increasing film thickness.

The mass transfer of indoor particulate matter is independent of organic pollutants. The distributions of airborne particles and settled dust are primarily influenced by factors such as ventilation, particle deposition and resuspension. Thus, the concentration of indoor airborne particles ($TSP$, μg/m$^3$) is governed by Eq. (1).

$$V\frac{dTSP}{dt} = Q\left(P_p TSP_{out} - \mathrm{TSP}\right) - \sum v_{d,i} TSP A_i + \sum RM_i A_i \quad (1)$$

where, $V$ (m$^3$) is the volume of the room; $t$ (h) is the simulated time; $Q$ (m$^3$/h) is the air exchange rate of the room through natural ventilation; $P_p$ (unitless) is particle penetration factor; $TSP_{out}$ (μg/m$^3$) is the outdoor mass concentration of particles; the footnote, i, stands for the serial number of each indoor surface; $v_{d,i}$ (m/h) is the particle deposition velocity of the i$^{th}$ surface, the value of which is varied by the surface position; $A_i$ (m) is the area of the i$^{th}$ surface; $R$ (h$^{-1}$) is the particle resuspension rate; $M_i$ (μg/m$^2$) means the dust concentration on the i$^{th}$ surface. No indoor particle sources were assumed in the model.

The surface dust concentration, $M_i$, is coupled with airborne particle concentration, $TSP$, which can be determined by the mass balance formula, as shown in Eq. (2).

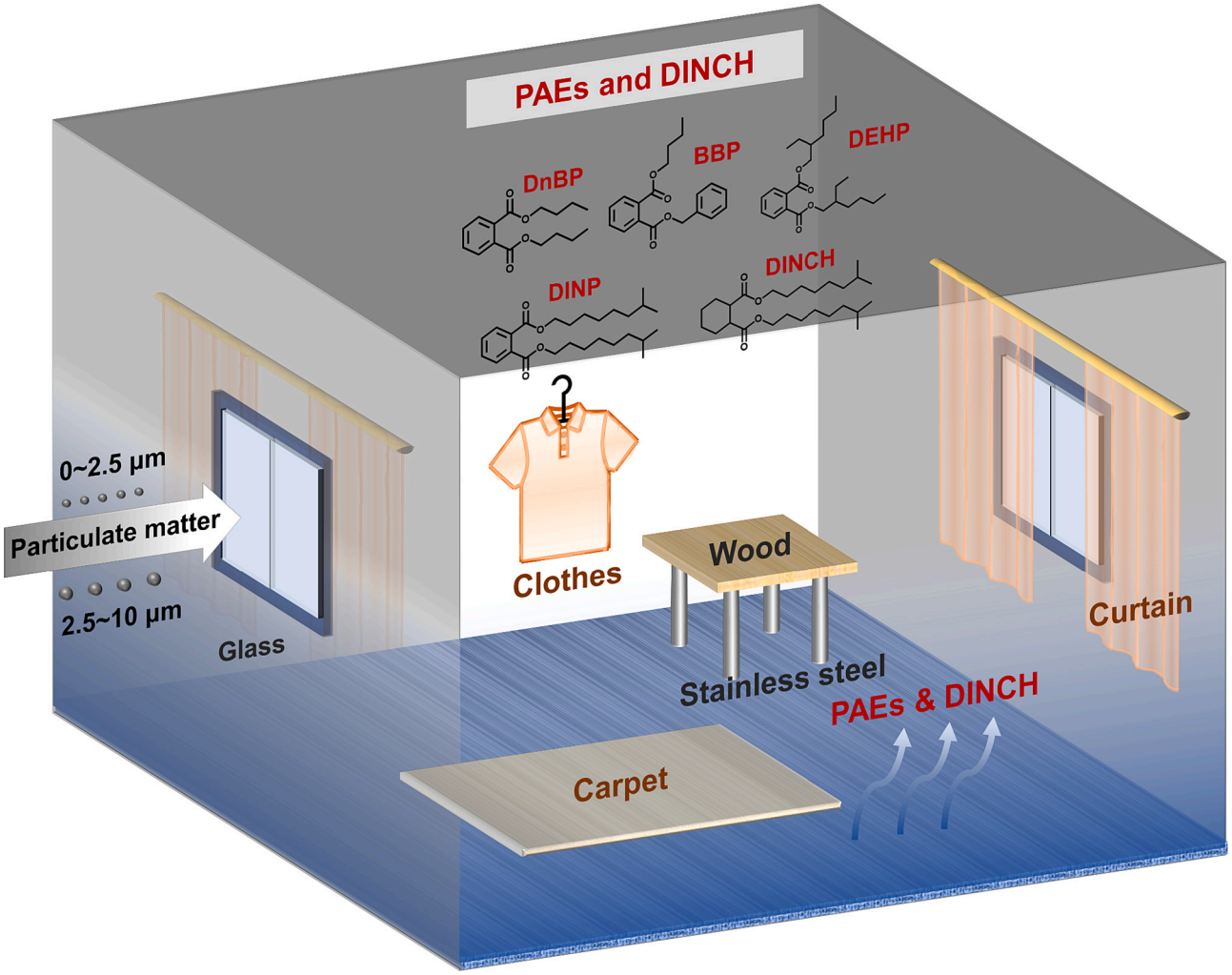


**Fig. 1.** Schematic of the mass transfer of SVOCs in indoor environments.

$$\frac{dM_i}{dt} = v_{d,i}TSP - RM_i \tag{2}$$

$PM_{2.5}$ and $PM_{2.5–10}$ are modeled separately based on Eqs. (1) and (2). The diameters of $PM_{2.5}$ and $PM_{2.5–10}$ are in the range of 0– 2.5 μm and 2.5– 10 μm, respectively. With the knowledge of particulate-matter distribution, SVOC concentration can be described based on the mass balance in the indoor environment. The mass transfer processes constrain the gas-phase SVOC concentrations via air exchange, emission from source surfaces, adsorption on non-source surfaces and release from airborne particles. Thus, the variation of gas-phase SVOC concentrations can be described by Eq. (3).

$$V\frac{dy}{dt} = Q(y_{out} - y) + h_{m,sur}A_s(y_0 - y) + \sum h_{m,sur}A_{ns,j}(y_{ns,j} - y) + \frac{3h_{m,p}TSP{\cdot}V}{\rho_p R_p}(y_p - y) \tag{3}$$

where, $y_{out}$ (μg/m$^3$) and $y$ (μg/m$^3$) are the outdoor and indoor gas-phase SVOC concentrations, respectively; $h_{m,sur}$ (m/h) and $h_{m,p}$ (m/h) are the mass transfer coefficient on indoor surfaces and airborne particles, respectively; the footnote, j, stands for the serial number of each non-source surface, which is different from the footnote, i, mentioned above; $A_s$ (m$^2$) and $A_{ns,j}$ (m$^2$) are the surface areas of source and the j$^{th}$ non-source surfaces; $y_0$ (μg/m$^3$), $y_{ns,j}$ (μg/m$^3$) and $y_p$ (μg/m$^3$) are the gas-phase SVOC concentration in boundary layers adjacent to the source, the j$^{th}$ non-source surfaces and airborne particles, respectively; $\rho_p$ (μg/m$^3$) and $R_p$ are the density and radius of the particulate matter, respectively. It is assumed no sources of the target SVOCs existed in the outdoor environments.

Considering the particle deposition and resuspension, particle-phase SVOC concentration, $F$ (μg/m$^3$), can be determined as shown in Eq. (4).

$$V\frac{dF}{dt} = Q(P_pF_{out} - F) + \frac{3h_{m,p}TSP{\cdot}V}{\rho_p R_p}(y - y_p) - \sum v_{d,i}FA_i + \sum RM_iA_iP_{dust,i} \tag{4}$$

where, $F_{out}$ (μg/m$^3$) and $F$ (μg/m$^3$) are the outdoor and indoor particle-phase SVOC concentrations, respectively; $P_{dust,i}$ (μg/g) is the dust-phase SVOC concentration loading on the i$^{th}$ surfaces. According to the definition, the parameter $y_p$ can be derived from $F$ (Weschler et al., 2008), shown in Eq. (5).

$$y_p = \frac{F}{K_p{\cdot}TSP} \tag{5}$$

where, $K_p$ (m$^3$/μg) is the partition coefficient of airborne particles.

As discussed by Xu and Little (2006), the SVOC-emission parameter ($y_0$) of source surfaces can be regarded as a constant, which could stay stable for several years, as testified by experimental and model analysis. The dust-phase SVOC concentration on the source surfaces, $P_{dust,s}$ (μg/g), can be regarded as a constant with the sorption equilibrium of $y_0$, which can be expressed as Eq. (6).

$$P_{dust,s} = K_{dust}y_0 \tag{6}$$

where, $K_{dust}$ (m$^3$/g) is the partition coefficient of settled dust.

Mass balances of SVOCs can also be established on indoor non-source surfaces to determine their concentrations in the dust and solid phases. The governing equation for SVOCs accumulating on the impermeable surface is shown as Eq. (7).

$$\frac{d(C_{ns,im} + M_{im}P_{dust,im})}{dt} = h_{m,sur}(y - y_{ns,im}) + v_dF - RM_{ns,im}P_{dust,im} \tag{7}$$

where, $C_{ns,im}$ (μg/m$^2$) is the surface SVOC concentration on the impermeable surfaces; $M_{im}$ (μg/m$^2$) and $P_{dust,im}$ (μg/g) are the surface dust concentration and dust-phase SVOC concentration, respectively. A linear relationship in SVOC partitioning among gas, settled dust and surface is assumed on the non-source surfaces according to Liang et al. (2019), as shown in Eq. (8).

$$y_{ns,im} = \frac{P_{dust,im}}{K_{dust}} = \frac{C_{ns,im}}{K_{ns,im}} \tag{8}$$

where $K_{ns,im}$ (m) is the partition coefficients of the impermeable surface. In this study, we modified the expression of $K_{ns,im}$ parameter to describe the organic-film growth along with the SVOC sorption. Details can be seen below in Section 2.2.

As for the permeable surfaces, SVOC sorption can be described as Eqs. (9) and (10).

$$\frac{\partial(C_{ns,p} + M_{p,x}P_{dust,p})}{\partial t} = \varepsilon D_a\frac{\partial^2 y_{ns,p}}{\partial x^2} \tag{9}$$

$$y_{ns,p} = \frac{P_{dust,p}}{K_{dust}} = \frac{C_{ns,p}}{\varepsilon + (1-\varepsilon)K_{ns,p}} \tag{10}$$

where, $C_{ns,p}$ (μg/m$^3$) and $y_{ns,p}$ (μg/m$^3$) are the solid-phase and gas-phase SVOC concentration on permeable surfaces, respectively; $M_{p,x}$ (μg/m$^3$) is the dust concentration at depth x in permeable materials; $\varepsilon$ (unitless) is the porosity; $D_a$ (m$^2$/h) is the mass diffusion of SVOC in the air; $K_{ns,p}$ (unitless) is the SVOC partition coefficient of the solid-phase permeable material. The boundary conditions of the permeable materials can be described as Eqs. (11)–(14) based on the indoor mass transfer model.

$$y_{ns,p} = 0, \quad t = 0 \tag{11}$$

$$\left.\frac{\partial(C_{ns,p} + M_{p,x}P_{dust,p})}{\partial t}\right|_{x=L} = 0, \quad t > 0 \tag{12}$$

$$\left.\frac{\partial(C_{ns,p} + M_{p,x}P_{dust,p})}{\partial t}\right|_{x=0} = h_{m,sur}\left(y - y_{ns,p}\big|_{x=0}\right) + v_dF - RM_{ns,p}P_{dust,p}\big|_{x=0}, \quad t > 0 \tag{13}$$

where, $L$ (m) is the thickness of the permeable material.

Moreover, the partition coefficients of airborne particles ($K_p$) and settled dust ($K_{dust}$) are supposed to be equal, based on the simplification of dust composition. According to Eqs. (1) and (2), the airborne particles can be exchanged with dust through deposition and resuspension. Thus, the airborne particles and dust are assumed to be composed of the same particulate matter with equivalent SVOC partition coefficients. We assume that SVOC is primarily absorbed into the organic films of particulate matter rather than adsorbing onto inorganic components, referring to Weschler and Nazaroff (2008). It is hypothesized that these organic films exhibit a sorption capacity for SVOCs similar to that of octanol, as proposed by Weschler and Nazaroff (2010). The expression for calculating $K_p$ and $K_{dust}$ can then be derived by Eq. (14).

$$K_p = K_{dust} = \frac{f_{om,part}{\cdot}K_{oa}}{\rho_p} \tag{14}$$

where, $f_{om,part}$ (unitless) is the volume fraction of organic films on the particulate matter; $K_{oa}$ (unitless) is the SVOC partition coefficient of octanol. The mass transfer process of particulate matter and SVOCs shown in Fig. 1 can then be adequately described and simulated based on the models shown as Eqs. (1)–(14).

### 2.2. Boundary conditions on impermeable surfaces

As mentioned in the Introduction section, researchers have two different assumptions on the SVOC surface partitioning behaviors in the literature recently: 1) some researchers assumed that monolayer adsorption of SVOCs occurs on impermeable surfaces; 2) others believed that gas-phase SVOCs would absorb by the organic film that existed on the surface, further leading to continuous film growth. The two

assumptions were both widely applied in recent years. For example, Da Ros and Curran (2021) experimentally characterized the DEP partition coefficients on glass and aluminum surfaces following the first assumption. Weschler and Nazaroff (2017) conducted a modeling analysis to predict the SVOC distribution in organic films based on the second assumption. Thus, we tend to believe that both assumptions are reasonable under specific scenarios. This study aims to compare the organic film formation performances under different widely-used assumptions.

For the first assumption, the values of $K_{ns,im}$ are regarded as constants but differ for the impermeable surfaces with different textures. We summarized the reported $K_{ns,im}$ in the literature. Further, we explored the log-linear relationship between $K_{ns,im}$ and physicochemical properties of SVOCs for different surfaces (see Section S3 of the supplementary materials for details). Then, the $K_{ns,im}$ of SVOCs can then be calculated and summarized in Table S5. As for the second assumption, the $K_{ns,im}$ will vary over the film thickness, which tends to be dominated by the SVOC absorption in organic films. Details can be seen in Eqs. (15) and (16).

$$K_{ns,im} = \delta_{om} \cdot K_{om} \tag{15}$$

$$\delta_{om} = \delta_{initial} + \sum \frac{C_{ns,im,SVOC}}{\rho_{SVOC}} \tag{16}$$

where, $\delta_{om}$ (m) and $K_{om}$ (unitless) are the film thickness and partition coefficient of the organic films formed on impermeable surfaces; $\delta_{initial}$ (m) is the thickness of the quickly formed thin organic film in the indoor environment; $C_{ns,im,SVOC}$ (m) and $\rho_{SVOC}$ (m) are the surface concentration on the impermeable surface and density of the target SVOC.

In previous studies, the partition coefficients of organic films, $K_{om}$, were often assumed as octanol-air partition coefficients ($K_{oa}$) (named $K_{oa}$ assumption). The assumption has been widely applied in modeling studies (Beko et al., 2013; Little et al., 2012; Liu et al., 2012; Shi and Zhao, 2014; Weschler and Nazaroff, 2017). The $K_{oa}$ values of SVOCs were also summarized in Table S4. However, Chen et al. have experimentally testified that film components greatly influence the SVOC partition coefficients (Chen et al., 2022a). Thus, the film-octanol assumption may be less accurate in estimating SVOC concentration distributions. Referring to the experimental results and the adsorption energy calculated by molecular dynamics simulation of our previous study (Chen et al., 2022a), we originally developed an empirical formula to predict the SVOC partition coefficients of the realistic indoor organic film. The formula is presented as Eq. (17).

$$log\left(\frac{K_{om}}{K_{oa}}\right) = 5.53 \times log\left(\frac{E_{ad,om}}{E_{ad,octanol}}\right) - 1.12 \tag{17}$$

where, $E_{ad,om}$ (kcal/mol) and $E_{ad,octanol}$ (kcal/mol) are the adsorption energies of SVOC in realistic organic films and octanol films, respectively. The empirical formula is developed based on the results of toluene, hexanol and benzyl alcohol in DnBP and DEHP organic films given by Chen et al. (2022a), additional details of which can be found in Section S1 of the supplementary materials. The organic-film components are obtained referring to Liu et al. (2003), with the summarized results presented in Fig. S2a of the supplementary materials. The realistic organic films mainly include $C_nH_{2n+2}$ (C10 ~ 36, 9.9 %), $C_nH_{2n-2}O_4$ (C6 ~ 14, 9.9 %) and $C_nH_{2n}O_2$ (C11 ~ 31, 79.3 %) according to the field-test results. We can then calculate the $K_{om}$ of SVOCs by combining the empirical formula and simulated adsorption energy on realistic organic films. The $K_{om}$ values were summarized in Fig. S2b of the supplementary materials, the values of which range from 1.8 to 53.3 times as large as $K_{oa}$.

### 2.3. Scenarios and human exposure

The mass transfer model containing particular matters and SVOCs is applied to a representative residence in Beijing, China. The residence in the model is 65 $m^2$ in area and 2.8 m in height, according to the Beijing Municipal Bureau of Statistics (Shi and Zhao, 2012). The modeled residence consists of a living room with a kitchen (24.6 $m^2$), a hallway (8.3 $m^2$), two bedrooms (14 $m^2$ × 2) and a bathroom (4.1 $m^2$). Objects such as vinyl floorings, furniture, carpet, windows, fabrics and other small objects are set inside the rooms as SVOC source and non-source surfaces. Surface areas are estimated based on the method described by Hodgson et al. (2005) (refer to Section S2 of the supplementary materials for details). The indoor objects can be categorized into six types of materials, containing one source, three impermeable, and two permeable non-source materials. The primary source surface is vinyl flooring, which has been reported to contain a wide range of SVOCs in previous studies (Cao et al., 2016; Clausen et al., 2012; Eichler et al., 2018; Liang and Xu, 2014a; Liang and Xu, 2014b; Liang and Xu, 2015; Wu et al., 2016; Xie et al., 2016; Xu et al., 2012). An obvious positive correlation can be obtained between $y_0$ and mass fraction, $C_0$, of SVOC in vinyl flooring based on the reported data in the references, as shown in Table S3 of the supplementary materials. The $y_0$ values for DnBP, BBP, DEHP, DINP and DINCH are determined based on the linear relationships in Fig. S3 of the supplementary materials. The impermeable non-source surfaces include hardwood material, stainless steel and glass, while the permeable ones contain carpet and cloth. The classification of hardwood material as an impermeable surface and the wood partition coefficients are referred from the studies of Xu et al. (2009) and Liang et al. (2019). Although they did not explain the reason in the articles, we suppose it may be that the wood material indoors tends to be surface-treated to form a dense layer on surfaces. Considering the indoor positions of the target materials, we assume the vinyl flooring and carpet as upward-facing horizontal surfaces, and model the rest materials in both upward-facing horizontal and vertical positions. The upward-facing horizontal position is simplified as the horizontal position hereinbelow for the convenience of result presentation. Details can be seen in Section S2 of the supplementary materials.

The deposition velocities of $PM_{2.5}$ and $PM_{2.5–10}$ on the surfaces are then determined according to the locations, as shown in Table S2 of the supplementary materials. Meanwhile, the partition coefficients of non-source surfaces were summarized in Table S5 of the supplementary materials, and the mass transfer coefficients can be seen in Table S6 of the supplementary materials. The airborne particles are introduced into the indoor air through ventilation, the penetration ratios, $P_p$, of which are 0.8 and 0.3 for $PM_{2.5}$ and $PM_{2.5–10}$, respectively. The outdoor particle concentrations are determined by concentration probability densities calculated from the historical $PM_{2.5}$ and $PM_{2.5–10}$ data from December 5th 2013, to June 25th 2022, in Beijing (see Section S5 of the supplementary materials for details).

The influence on human exposure aggravations caused by SVOC combined sorption and film formation is also evaluated in this study. For this purpose, a 3-year-old child as the reference person is assumed to live in the modeled residence. Meanwhile, once-a-week cleanings are performed on indoor impermeable surfaces, carpets and cloth. The clean efficiencies of impermeable surfaces and carpets were set as 60 % and 22 %, respectively (Ewers et al., 1994). Since there was no reported clean efficiency of cloth in literature, we assumed the value as 80 % for cloth. The quantification of SVOC intakes involves three approaches: inhalation (gas and airborne particles), non-dietary ingestion (surface films and dust) and dermal absorption (gas, airborne particles and clothes). The SVOC inhalation intakes, $Expo_I$ (μg/kg/day), can be calculated by Eqs. (18)–(20).

$$Expo_{I,y} = \frac{y \times IR \times ED_{in}}{24 \times BW} \tag{18}$$

$$Expo_{I,F} = \frac{F \times IR \times ED_{in}}{24 \times BW} \tag{19}$$

$$Expo_{\mathrm{I}} = Expo_{\mathrm{I,y}} + Expo_{\mathrm{I,F}} \tag{20}$$

where, the $Expo_{\mathrm{I,y}}$ (μg/kg/day) and $Expo_{\mathrm{I,F}}$ (μg/kg/day) are inhalation exposure rates of gas-phase and particle-phase SVOCs, respectively; $IR$ ($m^3$/day) means the air-inhalation rate; $ED_{\mathrm{in}}$ (h/day) is the indoor exposure duration; $BW$ (kg) is the body weight of the reference people.

In modeling and field-test studies, dust intake is regarded as a non-dietary ingestion exposure (Beko et al., 2013; Bu et al., 2016; Gaspar et al., 2014). As described by the Exposure Factors Handbook, dust tends to be ingested through hand touching from surfaces to mouth (EPA, 2011). The organic films will be ingested simultaneously when the child touches the impermeable surfaces. We optimized the non-dietary ingestion exposure, $Expo_{\mathrm{NDI}}$ (μg/kg/day), and formulas referring to the studies on flame-retardant exposure assessment (Lim et al., 2014; Sugeng et al., 2020), as shown in Eqs. (21)–(23).

$$Expo_{\mathrm{NDI,dust}} = \frac{P_{\mathrm{dust}} \times IngR_{\mathrm{in}}}{BW} \tag{21}$$

$$Expo_{\mathrm{NDI,of}} = \frac{C_{\mathrm{ns,of}} \times f_{\mathrm{hand}} \times ED_{\mathrm{in}} \times A_{\mathrm{mouth}} \times R_{\mathrm{trans}}}{BW} \tag{22}$$

$$Expo_{\mathrm{NDI}} = Expo_{\mathrm{NDI,dust}} + Expo_{\mathrm{NDI,of}} \tag{23}$$

where, the $Expo_{\mathrm{NDI,dust}}$ (μg/kg/day) and $Expo_{\mathrm{NDI,of}}$ (μg/kg/day) are the non-dietary ingestion exposure rates of dust-phase and organic-film-phase SVOCs, respectively; $IngR_{\mathrm{in}}$ (g/day) is the dust intake rate; $f_{\mathrm{hand}}$ (times/day) is the frequency of touching the surface organic films; $A_{\mathrm{mouth}}$ ($m^2$) is the mouth area of the child; $R_{\mathrm{trans}}$ (dimensionless) is the transfer ratio from surface to mouth.

SVOCs reach the skin surfaces by mass transfer of the gas phase, deposition of particle phase and diffusion from clothes. Then, the SVOCs will infiltrate from skin surfaces through the stratum corneum/viable epidermis composite to dermal capillaries (Weschler and Nazaroff, 2012). The dermal absorption exposure, $Expo_{\mathrm{DA}}$ (μg/kg/day), can be calculated by Eqs. (24)–(27).

$$Expo_{\mathrm{DA,y}} = \frac{y \times k_{\mathrm{y}} \times SA \times f_{\mathrm{SA}} \times ED_{\mathrm{in}}}{24 \times BW}, \frac{1}{k_{\mathrm{y}}} = \frac{1}{h_{\mathrm{m,ss}}} + \frac{1}{k_{\mathrm{p,b}}} \tag{24}$$

$$Expo_{\mathrm{DA,F}} = \frac{F \times k_{\mathrm{F}} \times SA \times f_{\mathrm{SA}} \times ED_{\mathrm{in}}}{24 \times BW}, \frac{1}{k_{\mathrm{F}}} = \frac{1}{v_{\mathrm{d,ss}}} + \frac{1}{k_{\mathrm{p,b}}} \tag{25}$$

$$Expo_{\mathrm{DA,clothes}} = \frac{y_{\mathrm{ns,p,clothes}} \times k_{\mathrm{clothes}} \times SA \times (1 - f_{\mathrm{SA}}) \times ED_{\mathrm{in}}}{24 \times BW}, \frac{1}{k_{\mathrm{clothes}}} = \frac{L_{\mathrm{gap}}}{D_{\mathrm{a}}} + \frac{1}{k_{\mathrm{p,b}}} \tag{26}$$

$$Expo_{\mathrm{DA}} = Expo_{\mathrm{DA,y}} + Expo_{\mathrm{DA,F}} + Expo_{\mathrm{DA,clothes}} \tag{27}$$

where, $h_{\mathrm{m,ss}}$ (m/day) is the mass convection coefficient on skin surfaces; $k_{\mathrm{p,b}}$ (m/day) stands for the permeability coefficient describing the SVOC transport from skin surface to dermal capillaries; $v_{\mathrm{d,ss}}$ (m/day) is the particle deposition rate on skin surfaces; $SA$ ($m^2$) and $f_{\mathrm{SA}}$ are the total skin surface area and the fraction of the skin directly exposed to the air, respectively; $L_{\mathrm{gap}}$ (m) is the gap between the clothes and skin surfaces. We referred to the Exposure Factors Handbook by EPA (2011) for information on the reference people and exposure-evaluating parameters. Details can be seen in Table S7 of the supplementary materials.

## 3. Results and discussion

### 3.1. Model validation

We applied a field study as a criterion to validate the developed model in this study. We conducted a simulation on a case involving indoor BBP transport and compared the predicted results with the experimental results from a field study conducted by Bi et al. (2015a). The input parameters for the simulation were chosen based on the environmental parameters in Bi et al.'s study. The experimental research was conducted in a test house (six years after its construction), in which the emission and sorption kinetics of BBP were examined by determining the airborne- and dust-phase concentrations. The comparisons between the simulated and experimental results for airborne- and dust-phase BBP are shown in Fig. 2. The experimental results agree with the simulated curves for BBP in both the total airborne phase and dust phase on non-floors. BBP in the source-dust phase shows better agreement with the experimental results than in the non-source-dust phase, probably because of the inhomogeneous sampling dust on the non-source surfaces. On the other hand, there are relatively large deviations between the modeling and experimental results for the airborne-phase BBP, mainly due to the uncertainty of airborne particle concentrations in real indoor environments. In summary, the mass transfer model is verified as suitable for predicting the fate and transport of a single SVOC in indoor environments.

### 3.2. SVOC concentrations distribution

Based on the developed mass transfer model, we further calculated the SVOC concentration distributions in the indoor environments, setting the exposure time as 500 days. Here, we assumed organic films formed and SVOC combined sorption occurred on impermeable surfaces, the SVOC partition coefficients chosen as $K_{\mathrm{oa}}$ following the classic hypothesis of Weschler and Nazaroff (2008). No cleaning was applied in the indoor environment to explore the features of SVOC distributions in the gas phase, particle phase and on surfaces.

We first determined the airborne particle and dust concentrations, and the corresponding results are presented in Fig. S6 of the supplementary materials. The left y-axis data in Fig. S6 show the variations in the airborne particle concentrations over time. The airborne $PM_{2.5}$ concentration remains stable between 30 and 40 μg/$m^3$, close to $PM_{10}$ but much greater than $PM_{2.5-10}$. The results of indoor-airborne-particle concentrations agree well with previous field-test studies sampled in indoor environments, including hospitals (Wang et al., 2006), residences (Zhu et al., 2021) and underground garages (Zhao et al., 2017), in which the $PM_{2.5}$ occupied dominate proportions of $PM_{10}$ in airborne

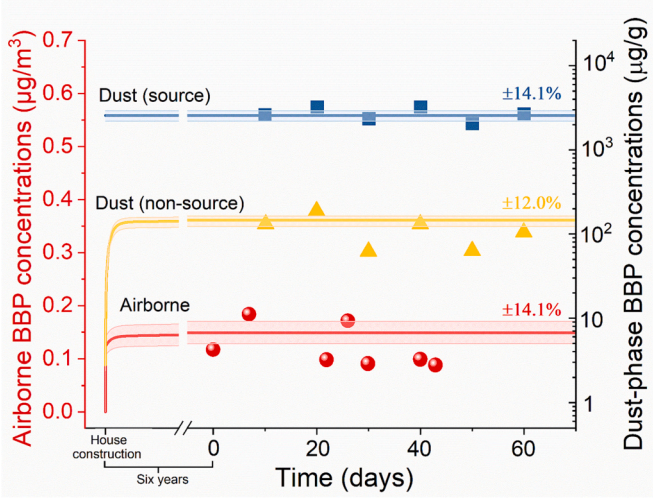


**Fig. 2.** Comparison of predicted BBP concentrations and the field-test results reported in Bi et al. (2015b). The red, yellow and blue lines represent the model-predicted results of the airborne phase, non-source-dust phase and source-dust phase, respectively. The shadows surrounding the lines indicate the error bars, which range from 12.0 % to 14.1 %, and result from the variability in the $y_0$ of source surfaces. The data points correspond to the experimental results from Bi's study with the same colors correlated with the lines.

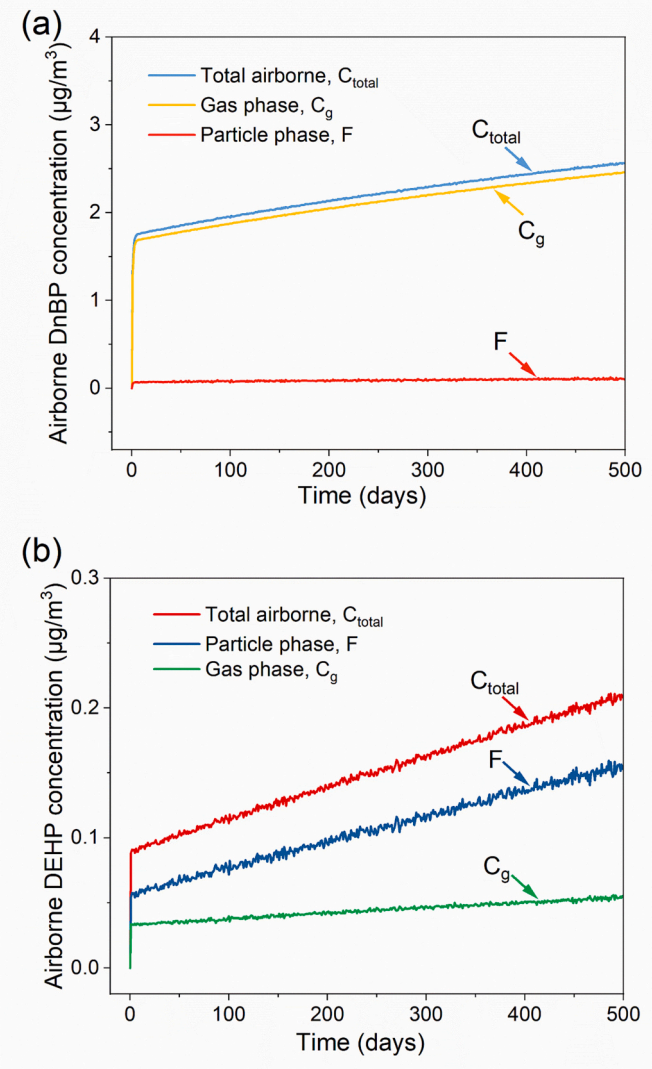


**Fig. 3.** The concentration distributions of (a) DnBP and (b) DEHP in the gas, particle and total airborne phase.

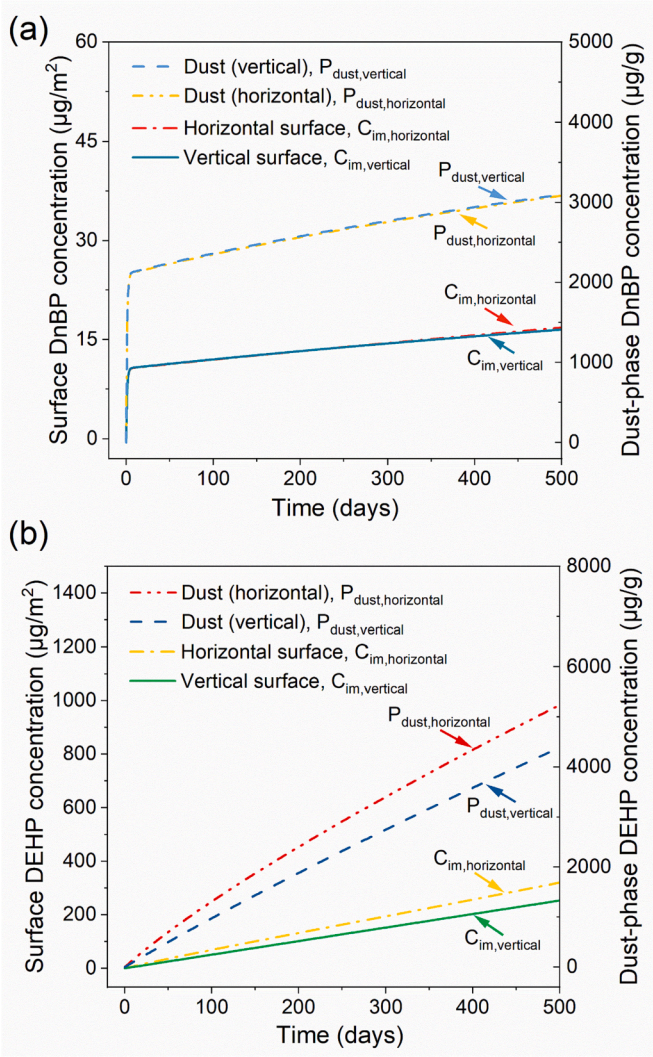


**Fig. 4.** The surface- and dust-phase concentration of (a) DnBP and (b) DEHP on impermeable surfaces at both horizontal and vertical positions. Concentrations of the surface phase (μg/m$^2$) were calculated for impermeable surfaces.

concentration. It indicates that $PM_{2.5}$ can exist stably in indoor air. $PM_{2.5–10}$ shows a smaller proportion of airborne particles due to its low permeation coefficient and large deposition rate (refer to Table S2 for details). The right y-axis data in Fig. S6 display the dust concentrations on the indoor upward-facing horizontal and vertical surfaces. A nearly linear-increasing tendency of surface dust concentrations over time is obtained during 500 days. The concentration-increasing velocities of horizontal surfaces are significantly larger than those of vertical surfaces. According to Eq. (2), surface dust concentrations are affected by the velocity of deposition ($v_d$) and resuspension ($R$), the former parameters of which differed largely for the surfaces with different positions, and the latter ones are the same (refer to Table S2 for details). Thus, the deposition velocity dominates the surface dust concentrations.

With the knowledge of particulate-matter distribution, the temporal and spatial variations of SVOC concentrations over time could be stimulated. We adopted DnBP and DEHP as the typical SVOCs to discuss the SVOC distribution characteristics in indoor environments. The results are shown in Figs. 3–5. The airborne concentrations in the gas and particle phase are shown in Fig. 3a and b for DnBP and DEHP, respectively. Due to the small molecular weight and sorption capacity, DnBP mainly exists in the gas phase, the concentrations of which increase to 1.8 μg/m$^3$ in several days and then lift at a slow velocity to 2.3 μg/m$^3$ at the end of 500 days. In comparison, as a large-molecular-weight SVOC, DEHP occupies significant proportions in particulate matter. DEHP concentrations in the particle phase increase linearly over time, reaching 0.15 μg/m$^3$ after a 500-day exposure. While, the gas-phase DEHP remains nearly stable at 0.04 μg/m$^3$ during 500 days. After the 500-day simulation, gas-phase DnBP concentration reached 37.2 % of the $y_0$ adjacent to the source material, while that of DEHP was no larger than 8.7 %. Considering the much larger partitioning capacity of DEHP than DnBP, DEHP tends to sorb on indoor interfaces when emitting from vinyl floorings instead of staying in the gas phase steadily. It should be noted that there is large variability in the total airborne, particle-phase and gas-phase DEHP concentrations shown in Fig. 3b. The source of data variability mainly resulted from the fluctuation of outdoor airborne particle concentration. According to the input parameters described in Section 2.3, SVOCs are leached from vinyl flooring and then adsorb on airborne particles in the indoor air. Meanwhile, the indoor airborne particle concentration is significantly affected by the outdoor concentration with large fluctuation, which is predicted by the concentration probability densities of outdoor $PM_{2.5}$ and $PM_{2.5–10}$ (see Section S5 of the supplementary materials for details). In contrast, the results of DnBP in Fig. 3a show less variability than DEHP, mainly due to the smaller sorption ability of DnBP on airborne particles. Thus, the fluctuation of airborne particle concentration has a minor impact on the airborne DnBP concentration.

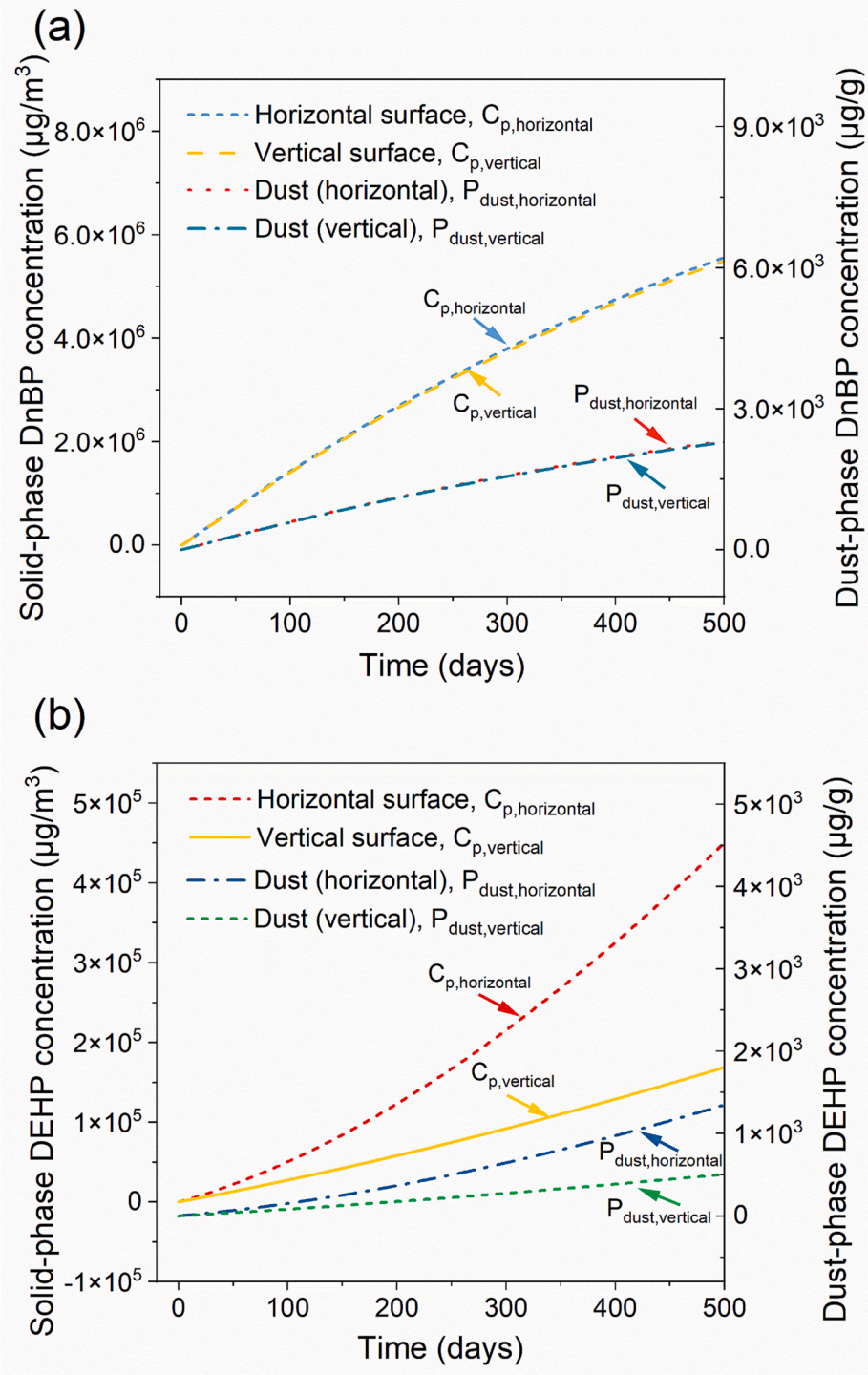


**Fig. 5.** The solid- and dust-phase concentration of (a) DnBP and (b) DEHP on permeable surfaces at both horizontal and vertical positions. Concentrations in the solid phase (μg/m$^3$) were calculated for permeable surfaces.

The surface- and dust-phase concentrations of DnBP and DEHP on impermeable surfaces are shown in Fig. 4a and b, respectively. Impermeable surfaces can be categorized at horizontal and vertical positions, and the SVOC concentration distributions were the same for different impermeable materials at the same position. The surface DnBP and DEHP concentrations showed continuous growth over time on both horizontal and vertical surfaces, in which the horizontal surface exhibited slightly larger DnBP concentrations and much larger DEHP concentrations. According to Eq. (7), the surface and dust-phase SVOC concentrations are governed by SVOC mass transfer in the gas phase as well as the deposition and resuspension in the particle phase, among which the mass transfer and particle resuspension are independent of surface positions. Airborne-particle deposition is the only factor differing for the surfaces with different positions. Thus, the larger deposition of particle-phase SVOC on horizontal surfaces leads to their continuous increases over time. Dust-phase DnBP concentrations are nearly the same for horizontal and vertical surfaces. In contrast, DEHP concentrations in horizontal-surface dust are relatively larger than those on vertical surfaces. Both the horizontal and vertical surfaces show linearly increasing tendencies for surface- and dust-phase SVOC

concentrations. In summary, DnBP shows similar surface- and dust-phase concentration distributions on the horizontal and vertical surfaces, while the surface and dust-phase DEHP concentrations accumulated on horizontal surfaces are significantly larger than those on horizontal surfaces. The large DEHP partition coefficients and particle-phase DEHP deposition rates on horizontal surfaces may be the key reasons leading to the larger surface and dust-phase DEHP concentrations on horizontal surfaces.

Significant differences exist in DnBP and DEHP concentration-increasing tendencies in permeable surfaces, as shown in Fig. 5a and b. Similar to impermeable surfaces, we also selected the permeable surfaces in horizontal and vertical positions for further discussion. The solid- and dust-phase DnBP concentrations were nearly the same for the surfaces at both horizontal and vertical positions. In contrast, both solid- and dust-phase DEHP concentrations in the horizontal positions are larger than those in the vertical position, which may be mainly due to the large particle deposition rates of horizontal surfaces and large partition coefficients of DEHP. Thus, it is supposed that the SVOCs with larger partition coefficients tend to be more significantly accumulated on the surfaces at horizontal positions. It should be noted that the concentrations of DnBP in permeable surfaces and settled dust increase continuously with decreasing velocities. As a comparison, the growth rates of DEHP concentrations in permeable material and dust show accelerated increases over time, indicating a gradual enhancement of DEHP mass transfer fluxes from indoor air to permeable surfaces. At the end of 500-day exposure, the DEHP concentration in horizontal permeable material is more than twice larger than the value in vertical one. According to Fig. 3b, the airborne DEHP mainly exists in the particle phase, which revealed an increasing tendency over time. Therefore, the increasing particle-phase DEHP concentration and deposition rates dominate the increasing DEHP concentration growth of solid and dust phases on horizontal surfaces.

### 3.3. Organic film formation

Based on the SVOC concentration distributions on impermeable surfaces in Section 3.2, it is found that surface DnBP and DEHP concentrations exhibit continuous growth over time. We further explored the film formation performances on impermeable surfaces with horizontal and vertical positions. The film formation performances of the constant $K_{ns,im}$ assumption, $K_{oa}$ assumption and $K_{om}$ assumption on impermeable surfaces can be seen in Fig. 6. In brief, the constant $K_{ns,im}$ assumption regarded the partition coefficients on impermeable surfaces as constants, in which the hardwood material was chosen as the target material for further discussion. The $K_{oa}$ assumption supposed octanol films covering impermeable surfaces, the film partition coefficients hypothesized as $K_{oa}$. In contrast, the $K_{om}$ assumption developed in this study applied the estimated $K_{om}$ of the realistic indoor organic films (refer to Section S1 of the supplementary materials for details).

After a 500-day SVOC continuous exposure, the organic film thickness increases nearly by 0.4 nm on both horizontal and vertical surfaces under the constant $K_{ns,im}$ assumption (Fig. 6a and b). In this case, there are upper limits for the surface SVOC sorption due to the constant source SVOC concentrations ($y_0$) and surface partition coefficients ($K_{ns,im}$). It is supposed to reach SVOC sorption balances on the surfaces, considering no further film increases after long-term exposure.

As for the cases under $K_{oa}$ assumption, the organic films show a nearly linear increase on the surface, indicating a different film

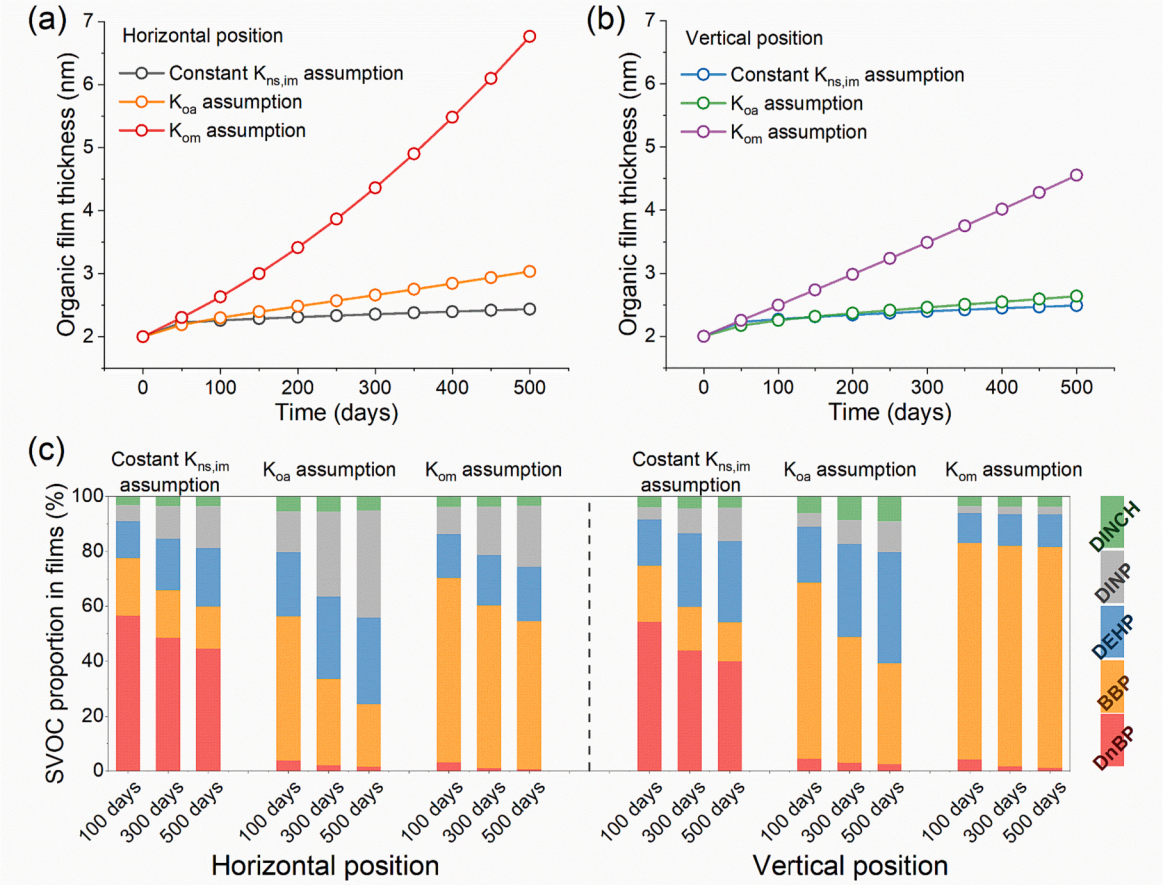


**Fig. 6.** Organic film formation performances on impermeable surfaces at (a) horizontal and (b) vertical positions under the constant $K_{ns,im}$ assumption, $K_{oa}$ assumption and $K_{om}$ assumption, respectively; (c) The SVOC proportions in organic films of the cases with different surface positions and film formation assumptions for 100, 300 and 500 days.

formation mechanism from the constant $K_{ns,im}$ assumption. The film thicknesses finally reached 3.03 nm and 2.64 nm for the horizontal and vertical surfaces, respectively, after being exposed to SVOCs for 500 days. The modeling results agree well with the field-test study of Huo et al. (2016), in which the organic films were continuously formed on windows under an approximately linear velocity over time. In this case, the airborne SVOCs tend to absorb in organic films, similar to dissolving in the organic solvent. Enriching one single SVOC would dilute the others' liquid-phase concentrations, resulting in a smaller gas-phase SVOC concentration adjacent to organic films according to the gas-liquid phase equilibrium principle (Chen et al., 2022a). Thus, there would be a continuous SVOC mass-transfer driving potential from air to organic films, leading to an increase in film thickness. The film thickness on the horizontal surface is nearly half larger than on the vertical surface. As it is described in Eq. (7), the SVOC mass transfer is mainly governed by the convection of the gas phase, the deposition of the airborne-particle phase and the resuspension of the dust phase, in which the deposition is the only factor affected by surface position. Thus, the larger particle deposition velocity of horizontal surfaces results in significant film-increasing performances.

When applying the partition coefficients of the realistic indoor organic films ($K_{om}$) in this model, the organic films exhibit significant growths with accelerating rates. The accelerating growth of organic films may lie in two critical factors: the continuously increasing film partition coefficients and the large SVOC transfer flux on horizontal surfaces. Due to the multiple SVOCs combined sorption in organic film, the organic film continuously grows, and the film partition coefficients are then increased. Meanwhile, the horizontal position of the surface results in a large deposition rate of particle-phase SVOCs to provide a large mass transfer flux to the horizontal surface. Thus, SVOCs in the airborne phase can then be consistently enriched in horizontal surfaces to enhance organic film growth and further lead to larger film partition coefficients. After a 500-day SVOC exposure, the films reach 6.76 nm and 4.55 nm in thickness for the horizontal and vertical surfaces, the former nearly half larger than the latter. Compared with $K_{oa}$, the $K_{om}$ are 1.8– 53.3 times larger in values, which leads to nearly twice larger film formation performances under $K_{om}$ assumption. It indicates that the larger film partition coefficients would significantly enlarge the film growth. Due to the difference between octanol and realistic organic films in physicochemical properties, the SVOC partition coefficients in realistic indoor organic films are well worth further quantified, considering their critical effects on film formation performances.

The SVOC proportions in organic films of the cases with different surface positions and film formation assumptions were calculated and shown in Fig. 6c. Across all six cases presented in Fig. 6c, obvious tendencies can be seen that the proportions of small-partition-coefficient SVOCs (DnBP and BBP) decrease over time, while those of large-partition-coefficient SVOCs (DEHP and DINP) enlarge. The result agrees well with the study of Weschler and Nazaroff (2017), which indicates that the partition coefficients of the dominant SVOCs in films increase over the exposure time. For the cases under $K_{oa}$ assumption, the components with the largest amounts are DINP and DEHP on horizontal and vertical surfaces after the 500-day exposure, respectively. In comparison, BBP occupied the largest proportion of horizontal and vertical surfaces under the $K_{om}$ assumption. The larger $K_{om}$ of BBP than $K_{oa}$ may be the key reason for more BBP accumulated in organic films for the cases under $K_{om}$ assumptions.

It should be noted that the organic films under the $K_{om}$ assumption accumulate more SVOCs in mass than the $K_{oa}$ assumption for both horizontal and vertical surfaces (Fig. 6a and b). According to Eq. (7), the SVOC mass transfers from air to organic films are limited to air convection, particle deposition, and resuspension, independent of the film partition coefficients. The performances of the SVOC-mass-transfer pathways are similar to both $K_{oa}$ and $K_{om}$ assumptions. Therefore, it is supposed that the larger partition coefficients do not enlarge the mass transfer fluxes to surfaces but change the SVOC distributions between organic films and the dust phase on the surfaces. In order to testify the inference, we further summarized the variation ratios of organic-film- and dust-phase SVOC concentrations of $K_{oa}$ and $K_{om}$ assumptions, compared with the data of constant $K_{ns,im}$ assumption. The results for 100-day, 300-day and 500-day exposures can be seen in Table 1, in which the increasing and decreasing ratios are marked as orange and blue, respectively. An obvious tendency can be seen that the SVOC concentrations sorbed on surfaces increase significantly along with the decreases of dust-phase concentrations for both $K_{oa}$ and $K_{om}$ assumptions. This trend becomes more pronounced as the SVOC exposure duration lengthens. With the larger SVOC partition coefficients, the cases under $K_{om}$ assumptions exhibit even higher surface-phase concentrations and lower dust-phase concentrations of SVOCs than those under $K_{oa}$ assumptions. This finding confirms that the variation of the surface partition coefficients influences the SVOC distribution between the surface and dust. When exposed to SVOCs for 500 days, there are nearly 2– 35 times increases in the surface SVOC concentrations except for DnBP on horizontal surfaces under $K_{om}$ assumptions, while the dust-phase SVOCs generally decrease nearly by 90 %. In contrast, the cases under $K_{oa}$ assumption result in much smaller increasing rates of surface-phase concentrations and decreasing rates of dust-phase concentrations (refer to Table 1 for details). Therefore, the film partition coefficient is the critical factor dominating the SVOC distributions between organic films and dust. The larger the film SVOC partition coefficient, the greater the transfer of SVOCs from settled dust to organic films.

### 3.4. Exposure assessment

The influences of SVOC film formation on child exposure were estimated in this section. We applied the once-a-week cleanings on the indoor environment, considering the human living conditions described in Section 2.3. The SVOC concentration distributions in airborne, surface and dust phases were calculated. DEHP was selected as the typical SVOC to exhibit the concentration variations under constant $K_{ns,im}$, film $K_{oa}$ and $K_{om}$ assumptions. The related results are summarized in Fig. S7. The DEHP concentrations vary in a similar tendency to the above assumptions. In brief, the gas- and particle-phase DEHP concentrations remain stable with slight fluctuations, while the DEHP concentrations in the surface and dust phases increase rapidly in the beginning and then hold stable with fluctuations in the frequency of indoor cleanings on indoor impermeable surfaces and clothes after 100 days. Thus, the SVOC-concentration distributions after 100 days in indoor environments were applied for the child exposure assessment.

We then calculated the SVOC uptakes of the 3-year-old child through inhalation, ingestion and dermal absorption. Three models describing SVOC sorption on impermeable surfaces containing constant $K_{ns,im}$, and film $K_{oa}$ and $K_{om}$ assumptions were applied to evaluate the film formations on human exposure. The results of SVOC uptakes by the child are shown in Fig. 7. The SVOC uptakes through ingestion range approximately from 10 to 100 μg/kg/day, which are 1– 4 orders of magnitude larger than those of inhalation and dermal absorption. The SVOC intakes of the child are <1 μg/kg/day through inhalation or dermal absorption, mainly due to the tiny SVOC amounts in the airborne phase and weekly-cleaned clothes. An obvious tendency can be seen that the SVOC-uptake amounts are increased through ingestion, and decreased through inhalation and dermal absorption along with the SVOC molecular weight increasing except for DINCH (Fig. 7a). A similar tendency can also be seen for the total SVOC uptake amounts shown in Fig. 7b, which are continuously enlarged over the SVOC molecular weight increasing (Fig. 7b). It should be noted that the DINCH do not follow the tendency as the other SVOCs (phthalates), which may be due to its distinct physicochemical property and low indoor concentration.

For the constant $K_{ns,im}$ and film $K_{oa}$ assumption models, dust-phase SVOC intakes occupy dominant proportions of ingestions, and the organic-film-ingestion proportions could approximately be neglected. In contrast, organic-film SVOC ingestions are significantly increased for the

**Table 1**
Variation ratios of surface- and dust-phase SVOC concentrations on impermeable surfaces under $K_{oa}$ or $K_{om}$ assumption compared with those under constant $K_{ns,im}$ assumption.

| Time | Variation ratio | DnBP | BBP | DEHP | DINP | DINCH | DnBP | BBP | DEHP | DINP | DINCH |
|---|---|---|---|---|---|---|---|---|---|---|---|
| | | $K_{oa}$ assumption | | | | | $K_{om}$ assumption | | | | |
| 100 days | $Sur_{horizontal}$ | 11.7% | 138.1% | 295.8% | 615.0% | 235.1% | 21.2% | 367.4% | 424.6% | 852.4% | 352.4% |
| | $Sur_{vertical}$ | 11.7% | 138.7% | 142.1% | 128.2% | 168.2% | 21.1% | 329.6% | 147.6% | 128.8% | 189.4% |
| | $Dust_{horizontal}$ | 101.3% | 88.7% | 41.8% | 34.4% | 48.4% | 101.2% | 4.1% | 3.4% | 3.7% | 5.2% |
| | $Dust_{vertical}$ | 101.3% | 89.6% | 18.3% | 4.6% | 34.1% | 101.2% | 3.8% | 1.1% | 0.4% | 2.8% |
| 300 days | $Sur_{horizontal}$ | 12.0% | 151.0% | 454.6% | 1063.6% | 340.0% | 23.1% | 1010.0% | 997.6% | 2172.2% | 801.1% |
| | $Sur_{vertical}$ | 11.9% | 149.0% | 209.9% | 169.1% | 275.0% | 22.4% | 850.3% | 233.3% | 170.9% | 381.7% |
| | $Dust_{horizontal}$ | 100.8% | 97.9% | 60.8% | 57.2% | 66.4% | 100.7% | 9.1% | 6.1% | 7.2% | 9.3% |
| | $Dust_{vertical}$ | 100.8% | 98.0% | 27.9% | 6.5% | 54.8% | 100.7% | 8.5% | 1.6% | 0.5% | 4.9% |
| 500 days | $Sur_{horizontal}$ | 12.4% | 155.6% | 548.6% | 1333.3% | 408.1% | 26.5% | 1685.3% | 1576.5% | 3491.5% | 1280.8% |
| | $Sur_{vertical}$ | 12.2% | 151.8% | 269.2% | 203.1% | 351.4% | 24.3% | 1329.0% | 317.9% | 205.9% | 582.5% |
| | $Dust_{horizontal}$ | 100.5% | 98.4% | 68.9% | 67.2% | 75.4% | 100.4% | 12.1% | 7.5% | 8.8% | 11.7% |
| | $Dust_{vertical}$ | 100.6% | 98.4% | 35.2% | 8.2% | 67.9% | 100.4% | 11.4% | 1.9% | 0.5% | 6.5% |
| <-100% | | | | | 0.0% | | | | | | >2000% |

Notes: Variation ratio of surface- and dust-phase SVOC following the formulas: $Sur_{im}=C_{ns,im,K}/C_{ns,im,con}$ or $Dust_{im}=Pdust_{ns,im,K}/Pdust_{ns,im,con}$, where the footprint, im, means the impermeable surfaces as hardwood material, steel, glass, wall and ceiling; the footprint, K, stand for the results under $K_{oa}$ or $K_{om}$ assumption, and the footprint, con, represented the results under the constant $K_{ns,im}$ assumption. The surface and dust-phase SVOC concentrations of the constant $K_{ns,im}$ assumption were calculated as the mean values of indoor impermeable surfaces.

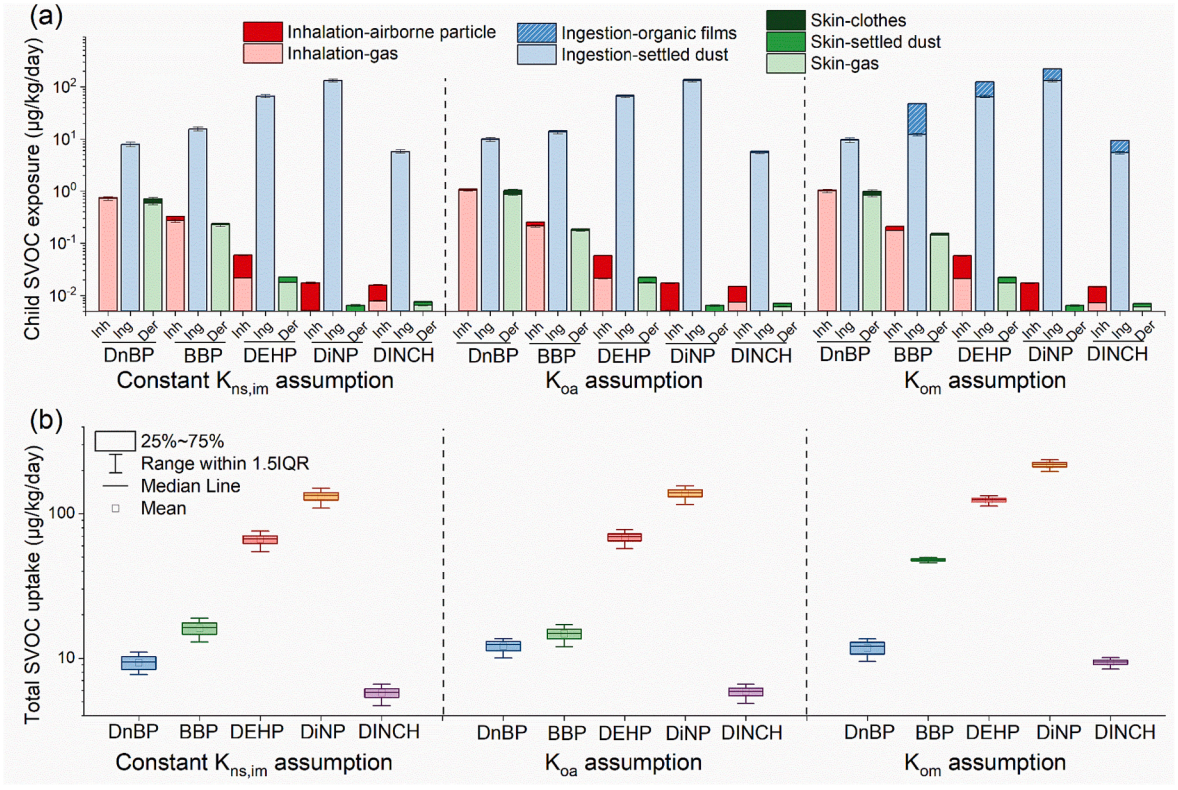


**Fig. 7.** The SVOC child-exposure assessments (a) through the pathways of inhalation, ingestion and dermal absorption and (b) of total uptake under the constant $K_{ns,im}$, $K_{oa}$ and $K_{om}$ assumptions.

cases under the $K_{om}$ assumption. The exposure-increasing ratios of BBP, DEHP and DINP under the $K_{om}$ assumption are 207.02 %, 87.6 % and 65.6 % for ingestion pathways and 198.7 %, 87.5 % and 65.6 % for the whole exposures, respectively, compared with the cases under the constant $K_{ns,im}$ assumption. Still, the $K_{om}$ assumption has a limitation in that the predicted partition coefficients of the realistic indoor organic films have not yet been experimentally verified. There are also some field studies focusing on the actual scenarios that surface-mouthing exposure contributes significant SVOC intake to humans (Chen et al., 2009; Eichler et al., 2021; Li et al., 2021; Lim et al., 2014; Stapleton et al., 2012; Sugeng et al., 2020). Chen et al. (2009) reported that children at the age between 3 and 36 months were evaluated to have much higher exposures of polybrominated diphenyl esters (PBDEs), a kind of SVOCs, than those aged 3–14 years, predominantly contributed through the surface-mouthing pathway. Stapleton et al. (2012) detected the PBDE amounts in serum were significantly correlated with those of handwipe ($p < 0.001$) of children, suggesting that hand-to-mouth activity may be a significant source of exposure to PBDEs. Lim et al. (2014) also discovered that 86 % of hand wipe samples detected significant amounts of PBDEs. Similar to PBDEs, Sugeng et al. (2020) found high detection amounts of organophosphorus esters on the surfaces of children's hands, which is associated with hand-to-object behavior. Based on the results of these studies, organic film ingestion is speculated to aggravate SVOC exposure through surface- and hand-mouthing. However, surface films are not the only contributor to SVOC uptake through the surface-mouthing pathway. Another important contributor is the settled dust adhered to surface films, which would be ingested by children simultaneously with organic films. Thus, more experimental evidence is required to substantiate the significance of the film ingestion pathway in SVOC exposure.

To better understand the film ingestion pathway of the case under $K_{om}$ assumption, we further explore the dominant source of the ingesting organic films. Thus, we calculated and summarized the proportion of organic film intakes from different indoor surfaces in Fig. S8 of the supplementary materials. The results show that the SVOC-organic-film intakes from the source vinyl floorings occupied >99.0 % except for DnBP (60.7 %), significantly larger than those of organic films on non-source impermeable surfaces. It indicates that the organic films formed on source surfaces are more hazardous and lead to large SVOC exposures to human beings. Considering the quickly-forming characteristics of initial thin films, SVOC exposures through organic film ingestion might be difficult to decrease through indoor cleanings. The phenomenon should be raised enough attention considering the potential exposures it brings to the undetermined indoor-source chemicals: the organic films covered on the so-called non-source material will result in large amounts of extra exposure if the material contains unknown organic pollutants. Therefore, organic film formation brings significant health risks to human beings and should be given more importance.

### 3.5. Limitations

This study's SVOC distributions and organic film formations are mechanistically estimated in the indoor environment exposed to multiple SVOCs. The exposure aggravations brought by film formations are also evaluated under different organic-film formation models. Nevertheless, some limitations remain to be refined in the future. We still simplified the indoor environments compared to the actual scenario, which contained more physical and chemical influences on the film formation. For example, we assumed the cleaning efficiency of organic film as a constant (60 %), referring to Ewers et al. (1994), and considered an approximate cleaning efficiency for cloth without further experimental validation. Meanwhile, we assumed that the organic film formed in the same position is uniform without considering the localized heterogeneity caused by UV-photo degradation and other effects. Experimental studies on the SVOC indoor removal are well worth further conducting. More importantly, the child's contact with film is also a film removal process, which is not considered in this study. In this study, the uniform assumption for the organic film is applied to the surfaces with the same positions. It is unable to analyze the influence of human touching based on localized film formations based on our current model. Therefore, a more refined SVOC mass transfer and film formation model is required for further research.

Besides indoor surfaces, organic films are also expected to form continuously on the particulate matter and then enlarge their volumes and SVOC partition coefficients. The phenomenon will result in larger amounts of SVOCs accumulated in airborne particles and settled dust, which remains to be verified in further modeling and experimental studies. Meanwhile, the SVOC partition coefficients in realistic indoor organic films, $K_{om}$, need further study. This study provides a $K_{om}$ predicting formula based on molecular dynamics simulation. However, the method requires further experimental certification. The SVOC partition coefficients are speculated to be varied along with the film components since the sorption was dominated by the molecular forces between molecules in the organic-film system (Ahmed and Jhung, 2017). Thus, a more elaborate model is expected to develop for the $K_{om}$ prediction. Moreover, only five types of SVOCs are applied as a case study to explore the SVOC combined sorption performances in this paper. As reported in previous research, there are many types and large amounts of SVOCs, including polycyclic aromatic hydrocarbons (PAHs), polychlorinated biphenyls (PCBs) and PBDEs, in indoor environments, which leads to a more complex sorption system (Weschler and Nazaroff, 2008). Therefore, SVOCs with larger amounts and more categories are expected to enrich indoor surfaces and dust and bring more health risks, which should be quantified in further work.

## 4. Conclusion

We conducted a modeling analysis on the combined sorption of multiple SVOCs in indoor environments to investigate the formation kinetics and child-exposure aggravations of SVOC organic films. Based on the model, organic film formation on the indoor surface can be delineated, and the exposure to the classical PAEs and DINCH in an actual scenario can be estimated. The results show that the SVOC concentration distributions in the gas phase, particle, surface and dust phase vary with SVOCs' physicochemical properties. Normally, SVOCs with small molecular weights mainly exist in the gas phase, exhibiting rapid variations in concentration over time. In contrast, SVOCs with large molecular weights tend to enrich in the particle, surface and dust phase with a slow increase in concentration. Compared with the convection of gas-phase SVOCs, the deposition of particle-phase SVOCs on surfaces is a more dominant factor in SVOC accumulation on indoor impermeable, permeable surfaces and dust, especially for the SVOCs with large molecular weights.

We further explored the performances of film formation on impermeable surfaces under three assumptions: the widely-used constant $K_{ns,im}$ assumption, $K_{oa}$ assumption, and the proposed $K_{om}$ assumption. The organic films under the $K_{oa}$ assumption are significantly thicker than those under constant $K_{ns,im}$ assumption. The organic films under the $K_{oa}$ assumption increase nearly linearly over time and agree well with the field-test study in tendency. Based on the $K_{oa}$ assumption, we applied molecular dynamics simulation to raise the partition coefficient prediction model for the realistic organic films ($K_{om}$). The film thicknesses estimated using the $K_{om}$ assumption are 2–3 times larger than those of the $K_{oa}$ assumption. It indicates that the film partition coefficient is the critical factor dominating the organic film formation, and the widely-used $K_{oa}$ assumption might underestimate the film-forming performances.

Finally, the SVOC exposure aggravations caused by organic-film formation for a 3-year-old child were evaluated by considering indoor surface cleaning. The analysis reveals that hazardous PAEs (BBP and DEHP) exhibit exposure-increasing ratios of 87.5 %–198.7 % due to organic-film ingestion under the $K_{om}$ assumption, compared to the

reference scenarios of $K_{ns,im}$ and $K_{oa}$ assumptions. Organic films formed on SVOC source surfaces are the key source of film SVOC intakes, occupying >99.0 %, except for DnBP (60.7 %). All in all, the formation of organic films presents potential health risks to humans and warrants greater attention.

## CRediT authorship contribution statement

**Jinhan Mo:** Conceptualization, Methodology, Funding acquisition, Writing - Review & Editing, Supervision.

**Zhuo Chen:** Experimental platform, Formal analysis, Resources, Data Curation, Writing - Original Draft, Writing - Review & Editing.

**Yilun Gao:** Visualization, Resources, Writing - Review & Editing.

**Fanxuan Xia:** Experimental platform, Writing - Review & Editing.

**Chenyang Bi:** Conceptualization, Writing - Review & Editing, Supervision.

## Declaration of competing interest

The authors declare that they have no known competing financial interests or personal relationships that could have appeared to influence the work reported in this paper.

## Data availability

Data will be made available on request.

## Acknowledgments

The research was supported by the National Key Research and Development Program of China (No. 2022YFC3702803) and the National Natural Science Foundation of China (Nos. 52078269 and 52325801).

## Appendix A. Supplementary data

Supplementary data to this article can be found online at https://doi.org/10.1016/j.scitotenv.2023.168970.

## References

Ahmed, I., Jhung, S.H., 2017. Applications of metal-organic frameworks in adsorption/separation processes via hydrogen bonding interactions. Chem. Eng. J. 310, 197–215. https://doi.org/10.1016/j.cej.2016.10.115.

Beko, G., Weschler, C.J., Langer, S., Callesen, M., Toftum, J., Clausen, G., 2013. Children's phthalate intakes and resultant cumulative exposures estimated from urine compared with estimates from dust ingestion, inhalation and dermal absorption in their homes and daycare centers. PloS One 8. https://doi.org/10.1371/journal.pone.0062442.

Bennett, D.H., Furtaw, E.J., 2004. Fugacity-based indoor residential pesticide fate model. Environ. Sci. Technol. 38, 2142–2152. https://doi.org/10.1021/es034287m.

Bi, C.Y., Liang, Y.R., Xu, Y., 2015a. Fate and transport of phthalates in indoor environments and the influence of temperature: a case study in a test house. Environ. Sci. Technol. 49, 9674–9681. https://doi.org/10.1021/acs.est.5b02787.

Bi, X.L., Yuan, S.J., Pan, X.J., Winstead, C., Wang, Q.Q., 2015b. Comparison, association, and risk assessment of phthalates in floor dust at different indoor environments in Delaware, USA. J. Environ. Sci. Health, Part A: Toxic/Hazard. Subst. Environ. Eng. 50, 1428–1439. https://doi.org/10.1080/10934529.2015.1074482.

Bolling, A.K., Sripada, K., Becher, R., Beko, G., 2020. Phthalate exposure and allergic diseases: review of epidemiological and experimental evidence. Environ. Int. 139, 105706 https://doi.org/10.1016/j.envint.2020.105706.

Bu, Z.M., Zhang, Y.P., Mmereki, D., Yu, W., Li, B.Z., 2016. Indoor phthalate concentration in residential apartments in Chongqing, China: implications for preschool children's exposure and risk assessment. Atmos. Environ. 127, 34–45. https://doi.org/10.1016/j.atmosenv.2015.12.010.

Cao, J.P., Weschler, C.J., Luo, J.J., Zhang, Y.P., 2016. Cm-history method, a novel approach to simultaneously measure source and sink parameters important for estimating indoor exposures to phthalates. Environ. Sci. Technol. 50, 825–834. https://doi.org/10.1021/acs.est.5b04404.

Chen, S.J., Ma, Y.J., Wang, J., Chen, D., Luo, X.J., Mai, B.X., 2009. Brominated flame retardants in children's toys: concentration, composition, and children's exposure and risk assessment. Environ. Sci. Technol. 43, 4200–4206. https://doi.org/10.1021/es9004834.

Chen, Z., Chen, Q., Xu, Y., Mo, J., 2022a. Partitioning characteristics of indoor VOCs on impermeable surfaces covered by film-phase DnBP and DEHP. J. Hazard. Mater. Adv. 8, 100191 https://doi.org/10.1016/j.hazadv.2022.100191.

Chen, Z., Wu, Q., Xu, Y., Mo, J., 2022b. Partitioning of airborne PAEs on indoor impermeable surfaces: a microscopic view of the sorption process. J. Hazard. Mater. 424, 127326 https://doi.org/10.1016/j.jhazmat.2021.127326.

Chen, Q., Tian, E., Wang, Y., Mo, J., Xu, G., Zhu, M., 2023. Recent progress and perspectives of direct ink writing applications for mass transfer enhancement in gas-phase adsorption and catalysis. Small Methods 7, 2201302. https://doi.org/10.1002/smtd.202201302.

Clausen, P.A., Liu, Z., Kofoed-Sørensen, V., Little, J., Wolkoff, P., 2012. Influence of temperature on the emission of di-(2-ethylhexyl)phthalate (DEHP) from PVC flooring in the emission cell FLEC. Environ. Sci. Technol. 46, 909–915. https://doi.org/10.1021/es2035625.

Da Ros, S., Curran, K., 2021. Modelling and parameter estimation of diethyl phthalate partitioning behaviour on glass and aluminum surfaces. Chemosphere 285, 131414. https://doi.org/10.1016/j.chemosphere.2021.131414.

Eichler, C.M.A., Wu, Y.X., Cao, J.P., Shi, S.S., Little, J.C., 2018. Equilibrium relationship between SVOCs in PVC products and the air in contact with the product. Environ. Sci. Technol. 52, 2918–2925. https://doi.org/10.1021/acs.est.7b06253.

Eichler, C.M.A., Cao, J.P., Isaacman-VanWertz, G., Little, J.C., 2019. Modeling the formation and growth of organic films on indoor surfaces. Indoor Air 29, 17–29. https://doi.org/10.1111/ina.12518.

Eichler, C.M.A., Hubal, E.A.C., Xu, Y., Cao, J., Bi, C., Weschler, C.J., Salthammer, T., Morrison, G.C., Koivisto, A.J., Zhang, Y., Mandin, C., Wei, W., Blondeau, P., Poppendieck, D., Liu, X., Delmaar, C.J.E., Fantke, P., Jolliet, O., Shin, H.-M., Diamond, M.L., Shiraiwa, M., Zuend, A., Hopke, P.K., von Goetz, N., Kulmala, M., Little, J.C., 2021. Assessing human exposure to SVOCs in materials, products, and articles: a modular mechanistic framework. Environ. Sci. Technol. 55, 25–43. https://doi.org/10.1021/acs.est.0c02329.

EPA, U.S, 2011. Exposure factors handbook, 20460. Office of research and Development, Washington, DC, pp. 2–6.

Ewers, L., Clark, S., Menrath, W., Succop, P., Bornschein, R., 1994. Cleanup of lead in household carpet and floor dust. Am. Ind. Hyg. Assoc. J. 55, 650–657. https://doi.org/10.1080/15428119491018736.

Fan, L.J., Wang, L.X., Wang, K.X., Liu, F., 2023. Phthalates in glass window films are associated with dormitory characteristics, occupancy activities and habits, and environmental factors. Environ. Sci. Pollut. Res. 30, 32550–32559. https://doi.org/10.1007/s11356-022-24536-x.

Fromme, H., Schutze, A., Lahrz, T., Kraft, M., Fernbacher, L., Siewering, S., Burkardt, R., Dietrich, S., Koch, H.M., Volkel, W., 2016. Non-phthalate plasticizers in German daycare centers and human biomonitoring of DINCH metabolites in children attending the centers (LUPE 3). Int. J. Hyg. Environ. Health 219, 33–39. https://doi.org/10.1016/j.ijheh.2015.08.002.

Gao, Y., Tian, E., Zhang, Y., Mo, J., 2022. Utilizing electrostatic effect in fibrous filters for efficient airborne particles removal: principles, fabrication, and material properties. Appl. Mater. Today 26, 101369. https://doi.org/10.1016/j.apmt.2022.101369.

Gao, Y., Tian, E., Mo, J., 2023. Electrostatic Polydopamine-Interface-Mediated (e-PIM) filters with tuned surface topography and electrical properties for efficient particle capture and ozone removal. J. Hazard. Mater. 441, 129821 https://doi.org/10.1016/j.jhazmat.2022.129821.

Gaspar, F.W., Castorina, R., Maddalena, R.L., Nishioka, M.G., McKone, T.E., Bradman, A., 2014. Phthalate exposure and risk assessment in California child care facilities. Environ. Sci. Technol. 48, 7593–7601. https://doi.org/10.1021/es501189t.

Golestanzadeh, M., Riahi, R., Kelishadi, R., 2020. Association of phthalate exposure with precocious and delayed pubertal timing in girls and boys: a systematic review and meta-analysis. Environ Sci Process Impacts 22, 873–894. https://doi.org/10.1039/c9em00512a.

Hodgson, A.T., Ming, K.Y., Singer, B.C., 2005. Quantifying Object and Material Surface Areas in Residences. Lawrence Berkeley National Lab.(LBNL), Berkeley, CA (United States). https://escholarship.org/uc/item/01b1h6sk.

Huo, C.Y., Liu, L.Y., Zhang, Z.F., Ma, W.L., Song, W.W., Li, H.L., Li, W.L., Kannan, K., Wu, Y.K., Han, Y.M., Peng, Z.X., Li, Y.F., 2016. Phthalate esters in indoor window films in a northeastern chinese urban center: film growth and implications for human exposure. Environ. Sci. Technol. 50, 7743–7751. https://doi.org/10.1021/acs.est.5b06371.

Lakey, P.S.J., Eichler, C.M.A., Wang, C., Little, J.C., Shiraiwa, M., 2021. Kinetic multi-layer model of film formation, growth, and chemistry (KM-FILM): boundary layer processes, multi-layer adsorption, bulk diffusion, and heterogeneous reactions. Indoor Air 31, 2070–2083. https://doi.org/10.1111/ina.12854.

Li, L., Westgate, J.N., Hughes, L., Zhang, X., Givehchi, B., Toose, L., Armitage, J.M., Wania, F., Egeghy, P., Arnot, J.A., 2018. A model for risk-based screening and prioritization of human exposure to chemicals from near-field sources. Environ. Sci. Technol. 52, 14235–14244. https://doi.org/10.1021/acs.est.8b04059.

Li, L., Hughes, L., Arnot, J.A., 2021. Addressing uncertainty in mouthing-mediated ingestion of chemicals on indoor surfaces, objects, and dust. Environ. Int. 146, 106266 https://doi.org/10.1016/j.envint.2020.106266.

Liang, Y.R., Xu, Y., 2014a. Emission of phthalates and phthalate alternatives from vinyl flooring and crib mattress covers: the influence of temperature. Environ. Sci. Technol. 48, 14228–14237. https://doi.org/10.1021/es504801x.

Liang, Y.R., Xu, Y., 2014b. Improved method for measuring and characterizing phthalate emissions from building materials and its application to exposure assessment. Environ. Sci. Technol. 48, 4475–4484. https://doi.org/10.1021/es405809r.

Liang, Y.R., Xu, Y., 2015. The influence of surface sorption and air flow rate on phthalate emissions from vinyl flooring: measurement and modeling. Atmos. Environ. 103, 147–155. https://doi.org/10.1016/j.atmosenv.2014.12.029.

Liang, Y.R., Bi, C.Y., Wang, X.K., Xu, Y., 2019. A general mechanistic model for predicting the fate and transport of phthalates in indoor environments. Indoor Air 29, 55–69. https://doi.org/10.1111/ina.12514.

Lim, Y.W., Kim, H.H., Lee, C.S., Shin, D.C., Chang, Y.S., Yang, J.Y., 2014. Exposure assessment and health risk of poly-brominated diphenyl ether (PBDE) flame retardants in the indoor environment of elementary school students in Korea. Sci. Total Environ. 470-471, 1376–1389. https://doi.org/10.1016/j.scitotenv.2013.09.013.

Little, J.C., Weschler, C.J., Nazaroff, W.W., Liu, Z., Hubal, E.A.C., 2012. Rapid methods to estimate potential exposure to semivolatile organic compounds in the indoor environment. Environ. Sci. Technol. 46, 11171–11178. https://doi.org/10.1021/es301088a.

Liu, Q.T., Chen, R., McCarry, B.E., Diamond, M.L., Bahavar, B., 2003. Characterization of polar organic compounds in the organic film on indoor and outdoor glass windows. Environ. Sci. Technol. 37, 2340–2349. https://doi.org/10.1021/es020848i.

Liu, C., Zhao, B., Zhang, Y., 2010. The influence of aerosol dynamics on indoor exposure to airborne DEHP. Atmos. Environ. 44, 1952–1959. https://doi.org/10.1016/j.atmosenv.2010.03.002.

Liu, C., Morrison, G.C., Zhang, Y., 2012. Role of aerosols in enhancing SVOC flux between air and indoor surfaces and its influence on exposure. Atmos. Environ. 55, 347–356. https://doi.org/10.1016/j.atmosenv.2012.03.030.

Liu, C., Deng, Y.L., Zheng, T.Z., Yang, P., Jiang, X.Q., Liu, E.N., Miao, X.P., Wang, L.Q., Jiang, M., Zeng, Q., 2020. Urinary biomarkers of phthalates exposure and risks of thyroid cancer and benign nodule. J. Hazard. Mater. 383 https://doi.org/10.1016/j.jhazmat.2019.121189.

Rodriguez-Carmona, Y., Ashrap, P., Calafat, A.M., Ye, X., Rosario, Z., Bedrosian, L.D., Huerta-Montanez, G., Velez-Vega, C.M., Alshawabkeh, A., Cordero, J.F., Meeker, J. D., Watkins, D., 2019. Determinants and characterization of exposure to phthalates, DEHTP and DINCH among pregnant women in the PROTECT birth cohort in Puerto Rico. J. Expo. Sci. Environ. Epidemiol. 30, 56–69. https://doi.org/10.1038/s41370-019-0168-8.

Schossler, P., Schripp, T., Salthammer, T., Bahadir, M., 2011. Beyond phthalates: gas phase concentrations and modeled gas/particle distribution of modern plasticizers. Sci. Total Environ. 409, 4031–4038. https://doi.org/10.1016/j.scitotenv.2011.06.012.

Shi, S., Zhao, B., 2012. Comparison of the predicted concentration of outdoor originated indoor polycyclic aromatic hydrocarbons between a kinetic partition model and a linear instantaneous model for gas–particle partition. Atmos. Environ. 59, 93–101. https://doi.org/10.1016/j.atmosenv.2012.05.007.

Shi, S., Zhao, B., 2014. Modeled exposure assessment via inhalation and dermal pathways to airborne semivolatile organic compounds (SVOCs) in residences. Environ. Sci. Technol. 48, 5691–5699. https://doi.org/10.1021/es500235q.

Shi, S., Zhao, B., 2015. Estimating indoor semi-volatile organic compounds (SVOCs) associated with settled dust by an integrated kinetic model accounting for aerosol dynamics. Atmos. Environ. 107, 52–61. https://doi.org/10.1016/j.atmosenv.2015.01.076.

Stapleton, H.M., Eagle, S., Sjödin, A., Webster, T.F., 2012. Serum PBDEs in a North Carolina toddler cohort: associations with handwipes, house dust, and socioeconomic variables. Environ. Health Perspect. 120, 1049–1054. https://doi.org/10.1289/ehp.1104802.

Sugeng, E.J., de Cock, M., Leonards, P.E.G., van de Bor, M., 2020. Toddler behavior, the home environment, and flame retardant exposure. Chemosphere 252, 126588. https://doi.org/10.1016/j.chemosphere.2020.126588.

Tian, E., Gao, Y., Mo, J., 2023. Experimental studies on electrostatic-force strengthened particulate matter filtration for built environments: progress and perspectives. Build. Environ. 228, 109782 https://doi.org/10.1016/j.buildenv.2022.109782.

Wang, X., Bi, X., Sheng, G., Fu, J., 2006. Hospital indoor PM10/PM2.5 and associated trace elements in Guangzhou, China. Sci. Total Environ. 366, 124–135. https://doi.org/10.1016/j.scitotenv.2005.09.004.

Wang, L.X., Zhao, A.Q., Wang, K.X., Liu, F., 2021. Phthalates in glass window films in university dormitories in Beijing, China, and exposure implications. Build. Environ. 196, 107813 https://doi.org/10.1016/j.buildenv.2021.107813.

Weschler, C.J., Nazaroff, W.W., 2008. Semivolatile organic compounds in indoor environments. Atmos. Environ. 42, 9018–9040. https://doi.org/10.1016/j.atmosenv.2008.09.052.

Weschler, C.J., Nazaroff, W.W., 2010. SVOC partitioning between the gas phase and settled dust indoors. Atmos. Environ. 44, 3609–3620. https://doi.org/10.1016/j.atmosenv.2010.06.029.

Weschler, C.J., Nazaroff, W.W., 2012. SVOC exposure indoors: fresh look at dermal pathways. Indoor Air 22, 356–377. https://doi.org/10.1111/j.1600-0668.2012.00772.x.

Weschler, C.J., Nazaroff, W.W., 2017. Growth of organic films on indoor surfaces. Indoor Air 27, 1101–1112. https://doi.org/10.1111/ina.12396.

Weschler, C.J., Salthammer, T., Fromme, H., 2008. Partitioning of phthalates among the gas phase, airborne particles and settled dust in indoor environments. Atmos. Environ. 42, 1449–1460. https://doi.org/10.1016/j.atmosenv.2007.11.014.

Wu, Y., Xie, M., Cox, S.S., Marr, L.C., Little, J.C., 2016. A simple method to measure the gas-phase SVOC concentration adjacent to a material surface. Indoor Air 26, 903–912. https://doi.org/10.1111/ina.12270.

Wu, Y.X., Eichler, C.M.A., Leng, W.N., Cox, S.S., Marr, L.C., Little, J.C., 2017. Adsorption of phthalates on impervious indoor surfaces. Environ. Sci. Technol. 51, 2907–2913. https://doi.org/10.1021/acs.est.6b05853.

Xie, M.J., Wu, Y.X., Little, J.C., Marr, L.C., 2016. Phthalates and alternative plasticizers and potential for contact exposure from children's backpacks and toys. J. Expo. Sci. Environ. Epidemiol. 26, 119–124. https://doi.org/10.1038/jes.2015.71.

Xu, Y., Little, J.C., 2006. Predicting emissions of SVOCs from polymeric materials and their interaction with airborne particles. Environ. Sci. Technol. 40, 456–461. https://doi.org/10.1021/es051517j.

Xu, Y., Hubal, E.A.C., Clausen, P.A., Little, J.C., 2009. Predicting residential exposure to phthalate plasticizer emitted from vinyl flooring: a mechanistic analysis. Environ. Sci. Technol. 43, 2374–2380. https://doi.org/10.1021/es801354f.

Xu, Y., Liu, Z., Park, J., Clausen, P.A., Benning, J.L., Little, J.C., 2012. Measuring and predicting the emission rate of phthalate plasticizer from vinyl flooring in a specially-designed chamber. Environ. Sci. Technol. 46, 12534–12541. https://doi.org/10.1021/es302319m.

Zartarian, V.G., Ferguson, A.C., Leckie, J.O., 1997. Quantified dermal activity data from a four-child pilot field study. J. Expo. Anal. Environ. Epidemiol. 7, 543–552. https://doi.org/10.1136/jech.51.5.579-a.

Zhang, X., Diamond, M.L., Ibarra, C., Harrad, S., 2009. Multimedia modeling of polybrominated diphenyl ether emissions and fate indoors. Environ. Sci. Technol. 43, 2845–2850. https://doi.org/10.1021/es802172a.

Zhang, X., Arnot, J.A., Wania, F., 2014. Model for screening-level assessment of near-field human exposure to neutral organic chemicals released indoors. Environ. Sci. Technol. 48, 12312–12319. https://doi.org/10.1021/es502718k.

Zhang, Q., Sun, Y., Zhang, Q., Hou, J., Wang, P., Kong, X., Sundell, J., 2020. Phthalate exposure in Chinese homes and its association with household consumer products. Sci. Total Environ. 719, 136965 https://doi.org/10.1016/j.scitotenv.2020.136965.

Zhao, Y., Song, X., Wang, Y., Zhao, J., Zhu, K., 2017. Seasonal patterns of PM10, PM2.5, and PM1.0 concentrations in a naturally ventilated residential underground garage. Build. Environ. 124, 294–314. https://doi.org/10.1016/j.buildenv.2017.08.014.

Zhu, Y., Fan, L., Wang, J., Yang, W., Li, L., Zhang, Y., Yang, Y., Li, X., Yan, X., Yao, X., Wang, X., 2021. Spatiotemporal variation in residential PM2.5 and PM10 concentrations in China: national on-site survey. Environ. Res. 202, 111731 https://doi.org/10.1016/j.envres.2021.111731.